EPJ Web of Conferences **146**, 04003 (2017) DOI: 10.1051/epjconf/201714604003
ND2016

Sensitivity of the ^{252}Cf(sf) neutron observables to the FREYA input yield functions $Y(A, Z, \mathrm{TKE})$

Jørgen Randrup[1,a], Patrick Talou[2], and Ramona Vogt[3,4]

[1] Nuclear Science Division, Lawrence Berkeley National Laboratory, Berkeley, California 94720, USA
[2] Nuclear Theory Group, Los Alamos National Laboratory, Los Alamos, New Mexico 87545, USA
[3] Nuclear and Chemical Sciences Division, Lawrence Livermore National Laboratory, Livermore, California 94551, USA
[4] Physics Department, University of California at Davis, Davis, California 95616, USA

Abstract. Within the framework of the fission event generator FREYA, we are studying the sensitivity of various neutron observables to the yield distribution $Y(A, Z, \mathrm{TKE})$ used as input to the code. Concentrating on spontaneous fission of ^{252}Cf, we have sampled a large number of different input yield functions based on χ^2 fits to the experimental data on $Y(A)$ and $Y(\mathrm{TKE}|A)$. For each of these input yield distributions, we then use FREYA to generate a large sample of complete fission events from which we extract a variety of neutron observables, including the multiplicity distribution, the associated correlation coefficients, and its factorial moments, the dependence of the mean neutron multiplicity on the total fragment kinetic energy TKE and on the fragment mass number A, the neutron energy spectrum, and the two-neutron angular correlation function. In this way, we can determine the variation of these observables resulting from the uncertainties in the experimental mesurements. The imposition of a constraint on the resulting mean neutron multiplicity reduces the variation of the calculated neutron observables and provides a means for shrinking the uncertainties associated with the measured data.

1. Introduction

In this study, we wish to ascertain how sensitive important neutron observables are to the specified input yield function $Y(A, Z, \mathrm{TKE})$. The general strategy is to consider an entire ensemble of possible yield functions that have been generated from the experimental data with due account taken of the associated uncertainties. For each such yield function, FREYA is used to generate a suitably large number of individual fission events from which the observables of interest are extracted. The resulting spread of these observables can then be regarded as a reflection of the original experimental uncertainties. The present report is a preliminary summary of a still ongoing study [1].

2. FREYA

Relative to the FREYA code described in the literature [2–7], we employ here a modified version that samples A, Z, and TKE directly from the input yield function $Y(A, Z, \mathrm{TKE})$. In the present preliminary study, the adjustable FREYA parameters $x, e_0, \mathrm{dTKE}, c_S$ are kept constant at nominal values in order to bring out the effect of the variation in the input yield functions $Y(A, Z, \mathrm{TKE})$. Consequently no attempt has yet been made to match the relatively well determined mean neutron multiplicity for each of the yield functions.

3. Yield functions

To generate a sample of yield functions, $\{Y^{(n)}(A, Z, \mathrm{TKE})\}$, we first perform a generalized least-square analysis of the various components that enter into the definition of the yields. A particular yield function is assumed to have the form

$$Y(A, Z, \mathrm{TKE}) = Y(A) \times P(Z \mid A) \times P(\mathrm{TKE} \mid A). \quad (1)$$

For each mass split, the TKE distribution is assumed to be of Gaussian form

$$Y(\mathrm{TKE} \mid A) \sim \exp\left(-[\mathrm{TKE} - \overline{\mathrm{TKE}}(A)]^2/2\sigma^2_{\mathrm{TKE}}(A)\right), \quad (2)$$

with $\int d\mathrm{TKE}\, Y(\mathrm{TKE} \mid A) = 1$. A least-square analysis of the available experimental data on $Y(A)$, $\overline{\mathrm{TKE}}(A)$, and $\sigma^2_{\mathrm{TKE}}(A)$ entering in Eqs. (1) and (2) was performed to obtained the mean distributions and their covariance matrices. Six experimental data sets were considered to obtain $Y(A)$ [8–13], six as well for $\overline{\mathrm{TKE}}(A)$ [10–15], and three for $\sigma^2_{\mathrm{TKE}}(A)$ [10–12]. Three experiments had particular influence on the resulting distribution: Göök and Hambsch [12], Hambsch and Oberstedt [11], and Budtz-Jørgensen and Knitter [10]. Those experiments also provided all three quantities from the same data set. No correlations between the different quantities were used in the present work. An example of the result of this statistical analysis work is shown in Fig. 1 for $\overline{\mathrm{TKE}}(A)$.

For a particular fragment mass, the charge distribution is obtained from Wahl systematics [16],

$$Y(Z \mid A) = \tfrac{1}{2} F(A, Z)\, N(A) \left[\mathrm{erf}(V^+) - \mathrm{erf}(V^-)\right] \quad (3)$$

[a] e-mail: JRandrup@LBL.gov

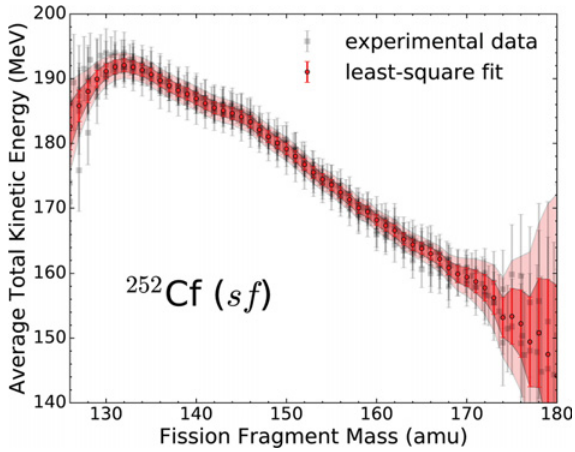

Figure 1. Experimental data (grey) and least-square evaluation (one-sigma, dark red; two-sigma, light red) of the average total kinetic energy TKE as a function of the fission mass split.

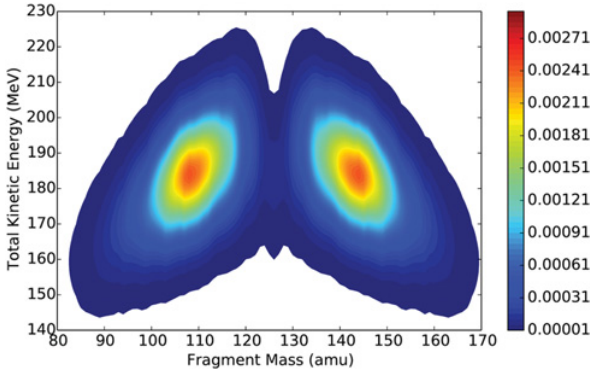

Figure 2. Contour plot of a 2D yield function $Y^{(ij)}(A, \mathrm{TKE}) = Y^{(i)}(A) \times \overline{\mathrm{TKE}}(A)^{(j)}$ obtained by the sampling procedure.

where $V^{\pm} = (Z - Z_p \pm \frac{1}{2})/(\sqrt{2}\sigma_z)$, $N(A)$ is a normalization factor ensuring $\int dZ\, P(Z \mid A) = 1$, and $F(A, Z)$ gives the odd-even staggering.

A Principal Component Analysis (PCA) [17] was then performed on each of the evaluated covariance matrices for each partial distribution in Eq. (1). The PCA decomposition leads to sampled realizations $Y(A)^{(i)}$, $\overline{\mathrm{TKE}}(A)^{(j)}$, and $\sigma^2_{\mathrm{TKE}}(A)^{(k)}$, and the sampled 3D yield functions $Y^{(n)}(A, Z, \mathrm{TKE})$ with $n = (ijk)$ then follow from (1). A particular realization of $Y(A, \mathrm{TKE})$ is shown in Fig. 2.

For a given channel, $(A_0, Z_0) \rightarrow (A_L, Z_L) + (A_H, Z_H)$, the Q-value, $Q_{LH} = M(A_0, Z_0) - M(A_L, Z_L) - M(A_H, Z_H)$, determines the total available excitation, $E^* = Q_{LH} - \mathrm{TKE}$, which is distributed (by FREYA) among the two fragments as rotational and statistical energy. Each of the fragments then undergo sequential neutron evaporation and the resulting product nuclei deexcite by photon radiation.

4. Results

We show here the effect on various neutron observables resulting from employing a sample of 1000 yield functions drawn from the distribution determined from available experimental data as described in Sect. 3. For each yield function, a total of one million events were generated.

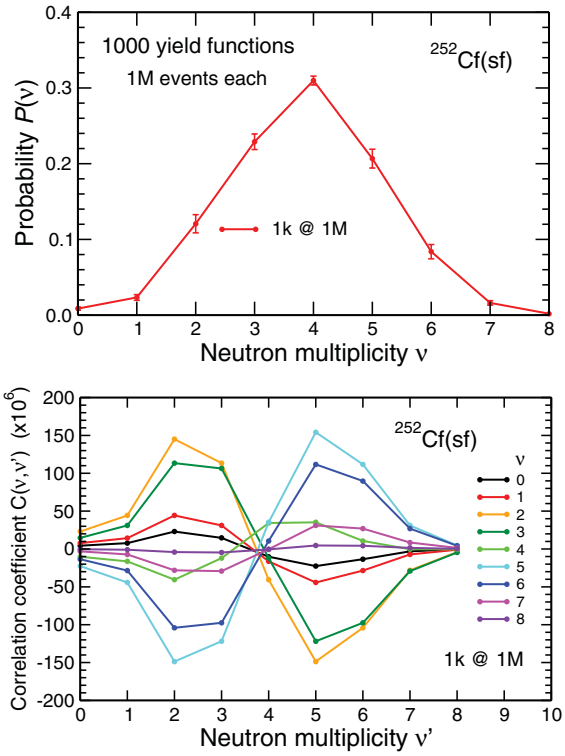

Figure 3. The neutron multiplicity distribution $P(\nu)$ (top) and the elements of the neutron multiplicity correlation matrix $C(\nu, \nu')$ shown as functions of ν' for the various values of ν (bottom) [18].

4.1. Multiplicity distribution

By analyzing 10^6 complete fission events for each of the N=1000 yield functions, $Y^{(n)}(A, Z, \mathrm{TKE})$, $n = 1, \ldots, N$, we determine the associated neutron multiplicity distribution, $P^{(n)}(\nu)$, for which we have

$$1 = \sum_{\nu \geq 0} P^{(n)}(\nu), \quad \bar{\nu}^{(n)} = \sum_{\nu \geq 0} \nu\, P^{(n)}(\nu) \tag{4}$$

where $\bar{\nu}^{(n)}$ is the mean neutron multiplicity resulting from the particular yield function $Y^{(n)}(A, Z, \mathrm{TKE})$.

The resulting mean multiplicity distribution, shown in Fig. 3 (top), is then

$$\langle P(\nu) \rangle \;=\; \frac{1}{N} \sum_{n=1}^{N} P^{(n)}(\nu) \tag{5}$$

and the associated covariance matrix (Fig. 3, bottom) is

$$C(\nu, \nu') = \frac{1}{N} \sum_{\nu} P^{(n)}(\nu)\, P^{(n)}(\nu') - \langle P(\nu) \rangle \langle P(\nu') \rangle. \tag{6}$$

An overall impression of the structure of the covariance matrix $C(\nu, \nu')$ can be gained from the contour plot in Fig. 4: Deviations from the average multiplicity at low ν are associated with opposite deviations at high ν.

A multiplicity distribution $P(\nu)$ can be characterized by its factorial moments,

$$\mathcal{M}_m \;\equiv\; \sum_{\nu \geq 0} \nu(\nu - 1) \cdots (\nu - m + 1)\, P(\nu). \tag{7}$$

These quantities were extracted for all the N multiplicity distributions, $\{ P^{(n)}(\nu) \}$, and Fig. 5 (top) shows the

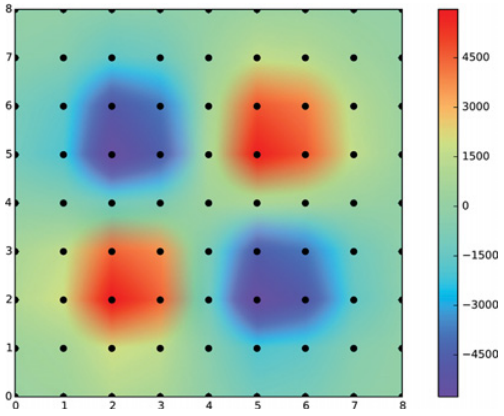

Figure 4. Contour plot of the covariance matrix shown in Fig. 3.

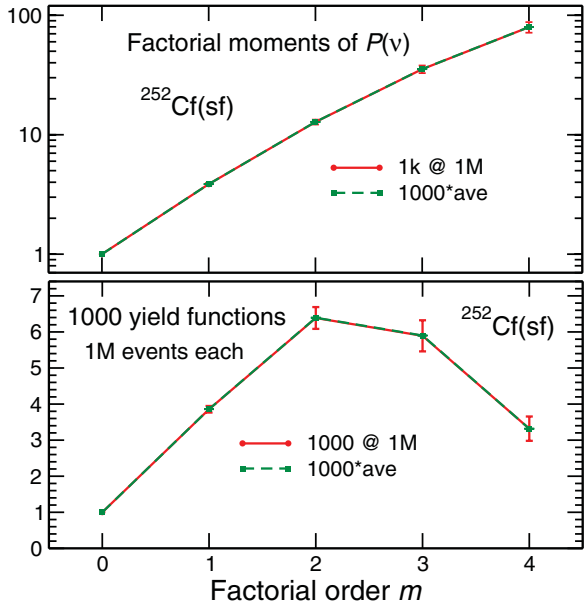

Figure 5. Top: factorial moments of the neutron multiplicity distribution, as obtained either from a sample of 1000 yield functions $Y(A, Z, \mathrm{TKE})$, with 10^6 events generated for each one (solid curve), or from reusing the average yield function 1000 times (dashed curve). Bottom: each factorial moment has been divided by $m!$ to eliminate the rapid growth with the order m [18].

resulting average values and the associated dispersions (indicated as error bars). Because the factorial moments tend to increase rapidly with the order m, it is preferable to divide each moment by $m!$, as shown in Fig. 5 (bottom).

Part of the dispersion obtained is due to the finite event sample (10^6) generated for each yield function and it is therefore important that the samples be sufficiently large. To verify that this is indeed the case, we have repeated the entire procedure using the same yield function all 1000 times (we used the average of the 1000 yield functions), in which case there is no effect on the extracted observables from a variation in the input to FREYA so all the entire dispersion is solely caused by the finite number of events. The corresponding results are included in Fig. 5 and subsequent figures (as dashed green curves). It is evident that the variance arising from the finite event sample is significantly smaller than the total variance, which can therefore be regarded as being well determined.

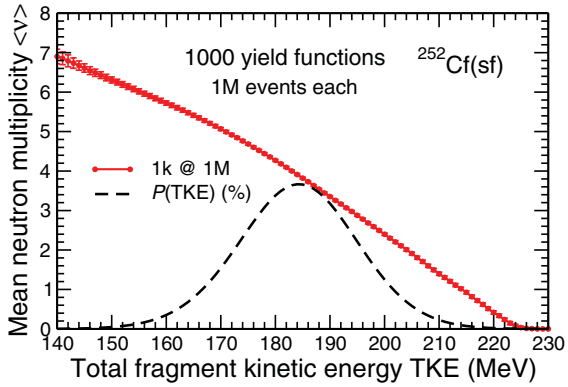

Figure 6. The dependence of the mean neutron multiplicity $\overline{\nu}$ on TKE, the total kinetic energy of the fission fragments, together with the TKE distribution (dashed curve) [18].

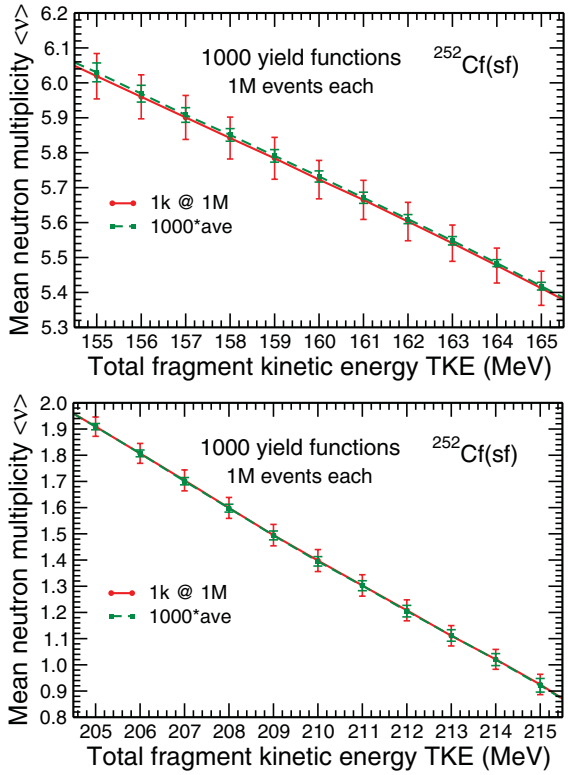

Figure 7. Magnified views of a low-TKE (top) and high-TKE (bottom) regions of $\overline{\nu}$(TKE) shown in Fig. 6 [18].

4.2. Dependence of multiplicity on TKE

Figure 6 shows the dependence of the mean neutron multiplicity $\overline{\nu}$ on the total kinetic energy of the two fission fragments. To better bring out the results, magnified views are shown in Fig. 7. Also here it is seen that the event sample size (10^6) is sufficient to give confidence in the extracted effects of the yield function variations.

Also shown on the same figure is the TKE distribution. It is apparent that the dispersions are rather small even for very small or very large TKE values where there are only relatively few events.

4.3. Dependence of multiplicity on mass

Figure 8 shows the dependence of the mean neutron multiplicity $\overline{\nu}$ on the fragment mass number A. To make the dispersions more visible, magnified views of $\overline{\nu}(A)$ are

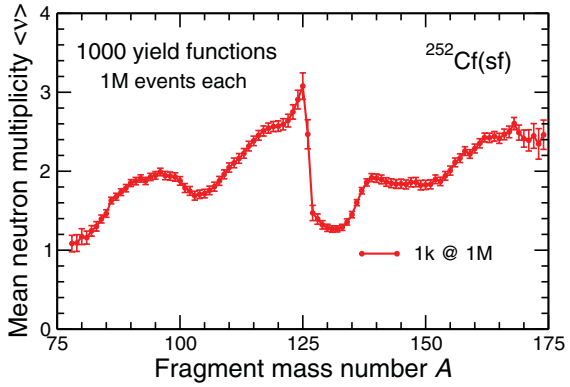

Figure 8. The mean neutron multiplicity $\overline{\nu}$ as a function of the fragment mass number A, $\overline{\nu}(A)$ [18]. Also for this observable, the effect from the finite number of events is negligible.

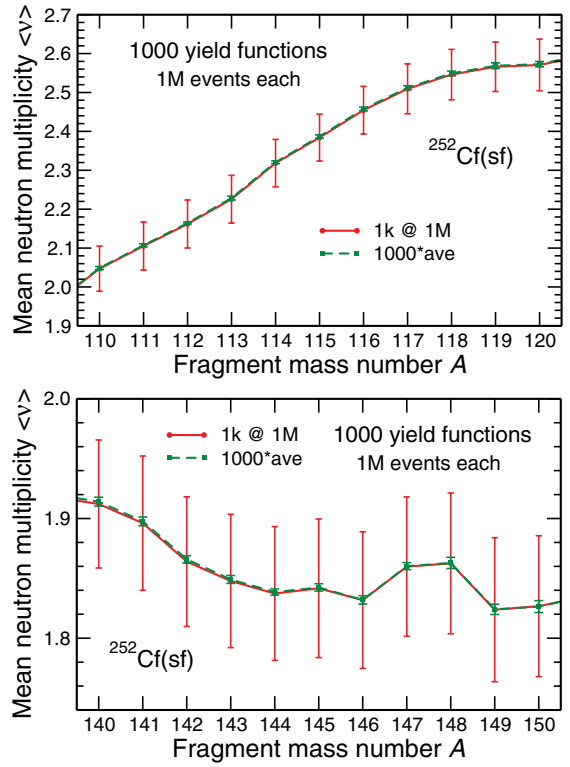

Figure 9. Magnified views of $\overline{\nu}(A)$ shown in Fig. 8 in the light (top) and heavy (bottom) mass regions [18]. (The error bars appear larger in the heavy-mass region only because the local flatness of $\overline{\nu}(A)$ permits a stronger magnification.)

shown in Fig. 9 for the light (A = 110–120) and heavy (A = 140–150) fragment mass regions. It is seen that the effect from the finite event sample is negligible.

We note again that for this preliminary study no attempt was made to fine tune the FREYA parameters in order to reproduce the experimental data not used as input, such as $\overline{\nu}(A)$ or the overall mean neutron multiplicity.

4.4. Spectral distribution

The spectral distribution of the evaporated neutrons, $F(E)\sim dv/dE$, is approximately of Maxwellian form (with $T\approx$1.42 MeV). With one million events, $F(E)$ can be sampled to a reasonable degree of accuracy out to $\approx$ 15 MeV. The effect of the uncertainty of the input yield

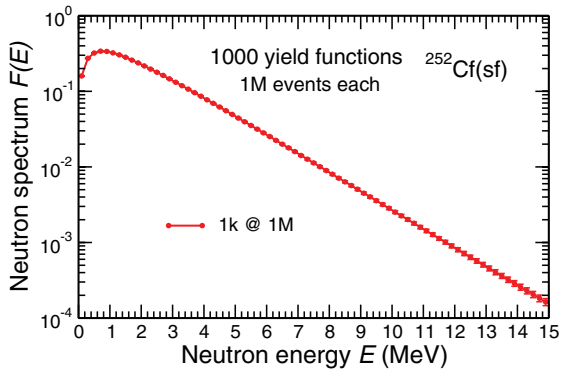

Figure 10. Spectral distribution of the evaporated neutrons [18].

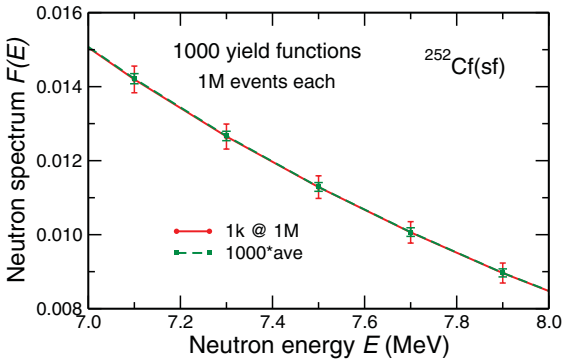

Figure 11. Magnified view of the spectral distribution $F(E)$ in the 7–8 MeV range of neutron kinetic energy [18].

function $Y(A, Z, \mathrm{TKE})$ on the spectral distribution of the evaporated neutrons is illustrated in Fig. 10.

On the logarithmic scale of Fig. 10 the effects are hardly visible and we therefore show a magnified view for neutrons in the region $E_\mathrm{n} = 7 - 8$ MeV (Fig. 11).

4.5. Angular correlations

Finally we examine the effect of the input variation on the neutron-neutron angular correlation function $C_\mathrm{nn}(\theta_{12})$.

The neutron-neutron angular correlations are rather insensitive to the input yields $Y(A, Z, \mathrm{TKE})$. That is because these angular correlations are dominated by the kinematic effects of the boost given to the evaporated neutrons by the moving fragments. As a consequence, $C_\mathrm{nn}(\theta_{12})$. does not depend much on the specific emitter fragments. Of greater importance is the ratio of neutrons emitted from the light and heavy fragments which is controlled in part by the FREYA parameter x,

5. Discussion

In this preliminary study we have, for spontaneous fission of ^{252}Cf, illustrated how the uncertainty in the input yield function $Y(A, Z, \mathrm{TKE})$, resulting from the inherent uncertainty in the experimental data, manifests itself in various neutron observables.

It is important to recognize that the procedure employed for determining the distribution of yield functions did not explicitly invoke the overall mean neutron multiplicity $\overline{\nu}$. As a consequence, the values of $\overline{\nu}$ obtained for the various sampled yield functions exhibit a variability that significantly exceeds the rather narrow

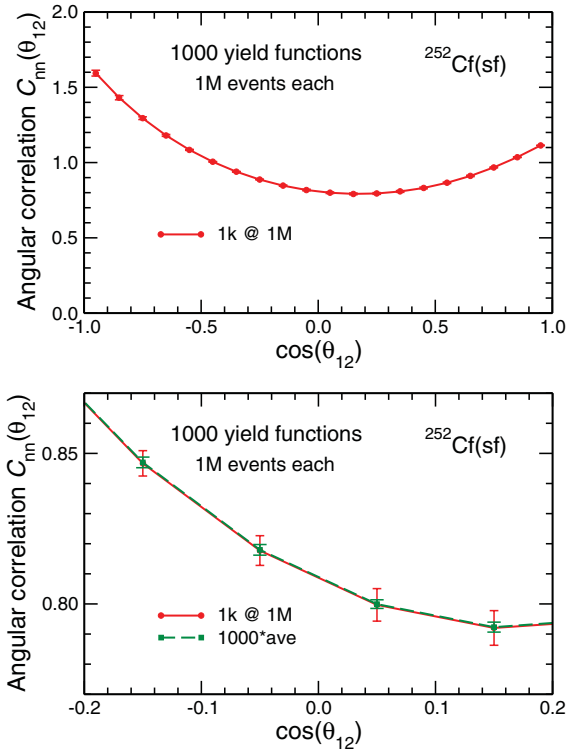

Figure 12. The angular correlation function over the entire angular range ($0^\circ \leq \theta_{12} \leq 180^\circ$), as a function of $\cos(\theta_{12})$ (top) and the angular correlation function in the central angular range ($\theta_{12} \approx 90^\circ$), as a function of $\cos(\theta_{12})$ (bottom) [18].

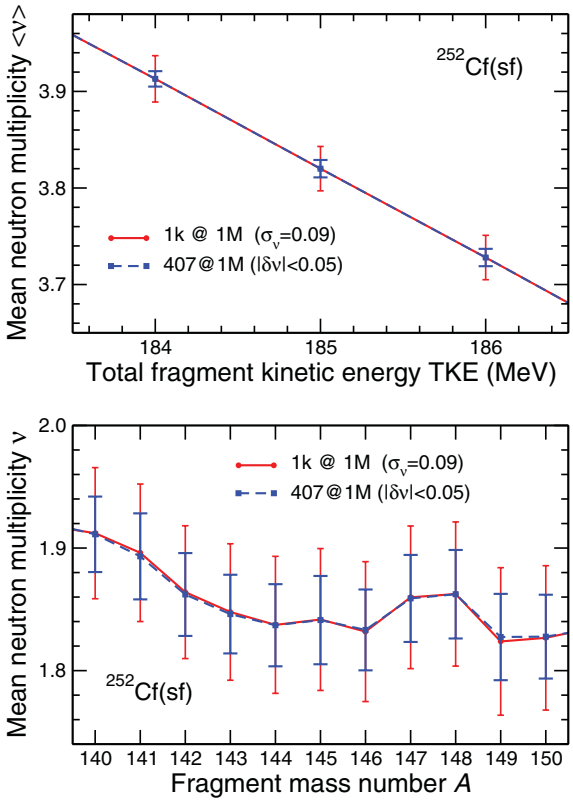

Figure 13. Effects of post-selecting the yield functions employed based on the resulting mean neutron multiplicity. This condition reduces the number of yield functions by a factor of around 0.4 and leads to smaller variations in the calculated observables [18].

experimental tolerance on this key quantity. It would therefore be preferable to consider yield functions that produce $\overline{\nu}$ values within the experimental range.

To elucidate the effect of such an additional constraint on the sample of yield functions, we have repeated the analysis for samples of yield functions obtained by retaining only those that lead to a mean neutron multiplicity within specified ranges.

The result is illustrated in Fig. 13 for the dependence of $\overline{\nu}$ on TKE. The retained yield functions are those that produce $\overline{\nu}$ values deviating less than 0.5 from the specifed target value (namely the overall mean multiplicity). While the multiplicities obtained with the unrestricted sample of 1000 yield functions have a dispersion of $\sigma_\nu \approx 0.09$, those resulting from the restricted sample (which consists of only 407 yield functions) have $\sigma_\nu \approx 0.03$. This is to be compared with the reported evaluated value for the standard deviation of the neutron multiplicity, $\sigma_\nu = 0.13\%$ [19], corresponding to $\sigma_\nu \approx 0.005$ which is six times smaller still.

It is clear from the plotted results, that the post selection leads to smaller variations in $\overline{\nu}$(TKE), as one would expect, but the shrinkage is considerably smaller than the factor of three by which the dispersion in $\overline{\nu}$ values is being reduced. This finding suggests that if the analysis were repeated for a sample of yield functions that all lead to $\overline{\nu}$ values lying within the experimental range, then the further reduction in the variation of the neutron observables would be relatively small. Such an analysis is underway.

We finally wish to note that ^{252}Cf(sf) is a special case (or an ideal test case) because the data we use to generate the input yield functions $Y(A, Z, \mathrm{TKE})$ are of good quality with high statistics. For all other actinides, with the possible exception of ^{235}U(n_{th},f) and ^{239}Pu(n_{th},f), the available input data are either not of as high quality or, in some cases, arise from models when no data are available at a given energy. Thus they do not provide as strong constraints on the yields and, therefore, not on the neutron observables either, as do those of ^{252}Cf(sf) which, as we have demonstrated here, are already insufficient to agree with the constraints on $\overline{\nu}$.

This work was supported in part by the Office of Defense Nuclear Nonproliferation Research & Development (DNN R&D), National Nuclear Security Administration in the U.S. Department of Energy. It was supported by the Office of Nuclear Physics in the U.S. Department of Energy's Office of Science under Contracts No. DE-AC02-05CH11231 (JR), DE-AC52-06NA25396 (PT), and DE-AC52-07NA27344 (RV), and by the U.S. National Science Foundation, Grant NSF PHY-0555660 (RV).

References

[1] J. Randrup, P. Talou, and R. Vogt, in preparation (2016)
[2] J. Randrup and R. Vogt, Phys. Rev. C **80**, 024601 (2009)
[3] R. Vogt and J. Randrup, Phys. Rev. C **84**, 044621 (2011)

[4] R. Vogt, J. Randrup, D.A. Brown, M.A. Descalle, and W.E. Ormand, Phys. Rev. C **85**, 024608 (2012)
[5] R. Vogt and J. Randrup, Phys. Rev. C **87**, 044602 (2013)
[6] R. Vogt and J. Randrup, Phys. Rev. C **90**, 064623 (2014)
[7] J. Randrup and R. Vogt, Phys. Rev. C **89**, 044601 (2014)
[8] C. Romano, Y. Danon, R. Block, J. Thompson, E. Blain, and E. Bond, Phys. Rev. C **81**, 014607 (2010)
[9] Sh. Zeynalov, F.-J. Hambsch, and S. Oberstedt, J. Korean Phys. Soc. **59**, 1396 (2011)
[10] C. Budtz-Jørgensen and H.-H. Knitter, Nucl. Phys. **A490**, 307 (1988)
[11] F.-J. Hambsch and S. Oberstedt, Nucl. Phys. **A617**, 347 (1997)
[12] A. Göök, F.-J. Hambsch, and M. Vidali, Phys. Rev. C **90**, 064611 (2014)
[13] E.M. Kozulin, A.A. Bogachev, M.G. Itkis, I.M. Itkis, G.N. Knyazheva, N.A. Kondratiev, L. Krupa, I.V. Pokrovsky, and E.V. Prokhorova, Inst. and Exp. Techniques **51**, 44 (2008)
[14] S.L. Whetstone, Jr., Phys. Rev. **131**, 1232 (1963)
[15] G.K. Mehta, J. Poitou, M. Ribrag, and C. Signarbieux, Phys. Rev. C **7**, 373 (1973)
[16] A.C. Wahl, Los Alamos Technical Report, LA-13298 (2002)
[17] M.E. Rising, A.K. Prinja, and P. Talou, Nucl. Sci. Eng. **175**, 188 (2013)
[18] The legend '1000@1M' on the calculated curves in Figs. 3 and 5–13 indicates that the results are based on 1000 sampled yield functions, for each of which one million complete fission events have been generated by FREYA; the legend '407@1M (—dν—¡0.05)' in Fig. 13 indicates that the results are based on the 407 yield functions for which the resulting average neutron multiplicity deviates less than 0.05 from the specified target value (namely the overall mean multiplicity). In Figs. 5, 7, 9, 11, 12 (bottom) the legend '1000*ave' indicates that the average yield function has been repeatedly used for a total of 1000 times (each time with a new sample of one million FREYA events)
[19] A.D. Carlson, V.G. Pronyaev, D.L. Smith, et al., Nucl. Data Sheets **110**, 3215 (2009)